Kawai, Shigeki; F. Canova, Filippo; Glatzel, Thilo; Hynninen, Teemu; Meyer, Ernst; Foster, Adam S.

Measuring Electric Field Induced Subpicometer Displacement of Step Edge Ions

Published in:
Physical Review Letters

DOI:
10.1103/PhysRevLett.109.146101

Published: 01/01/2012

Document Version
Publisher's PDF, also known as Version of record

Please cite the original version:
Kawai, S., F. Canova, F., Glatzel, T., Hynninen, T., Meyer, E., & Foster, A. S. (2012). Measuring Electric Field Induced Subpicometer Displacement of Step Edge Ions. *Physical Review Letters*, *109*(14), 1-5. Article 146101. https://doi.org/10.1103/PhysRevLett.109.146101

Measuring Electric Field Induced Subpicometer Displacement of Step Edge Ions

Shigeki Kawai,[1,*] Filippo Federici Canova,[2,3,†] Thilo Glatzel,[1] Teemu Hynninen,[2,3] Ernst Meyer,[1] and Adam S. Foster[2,3]

[1]*Department of Physics, University of Basel, Klingelbergstrasse 82, CH-4056 Basel, Switzerland*
[2]*Department of Physics, Tampere University of Technology, P.O. Box 692, FI-33010 Tampere, Finland*
[3]*COMP, Department of Applied Physics, Aalto School of Science, P.O. Box 11100, FI-00076 Aalto, Finland*

(Received 5 June 2012; published 3 October 2012)

We provide unambiguous evidence that the applied electrostatic field displaces step atoms of ionic crystal surfaces by subpicometers in different directions via the measurement of the lateral force interactions by bimodal dynamic force microscopy combined with multiscale theoretical simulations. Such a small imbalance in the electrostatic interaction of the shifted anion-cation ions leads to an extraordinary long-range feature potential variation and is now detectable with the extreme sensitivity of the bimodal detection.

DOI: 10.1103/PhysRevLett.109.146101 PACS numbers: 68.37.Ps, 34.20.Cf, 78.20.Bh

The measurement of potential variations near step edges is fundamental in surface physics, and unique quantum physical phenomena, such as a two-dimensional electron gas behavior, have been revealed on conductive surfaces by detailed studies on electrostatic potential variations with scanning tunneling spectroscopy, especially at low temperature [1–3]. Because of their high band gap, ionic crystal surfaces have recently attracted a lot of attention as a template for molecular electronic devices [4,5]. They have the advantage of electronically decoupling nanoobjects from the support [6,7] while offering the ability to tailor their properties [8–10]. The cleaved bulk surfaces often exhibit large and atomically flat terraces bounded by monoatomic step edges. In particular, the geometry and potential variations near step edges play a main role in growth and etching of crystals [11,12], adsorption of molecules [13–15] and metallic nanoclusters [16], including the diffusion and pinning dynamics of adsorbates [17,18], and friction [19,20]. It is well known that atomic interaction increases due to the low coordination of the step ions [21], forming an Ehrlich-Schwoebel-like barrier [22]. Furthermore, trapped local charges have been observed near step edges [23,24].

Because of their dielectric nature, dynamic force microscopy (DFM) is a suitable method to study ionic crystal surfaces at the atomic scale [25]. In DFM, the frequency shift Δf of an oscillating cantilever caused by the tip-sample interaction forces along the oscillation axis [26] is used for controlling the tip-sample separation while the tip scans the surface. The interpretation of DFM topographies is complicated due to the complexity of the imaging mechanism. In order to obtain better physical understanding, it is extremely useful to extract the site-dependent force from the measured Δf. Since the first systematic site-dependent dynamic force spectroscopy (DFS) measurement on Si(111) $-$ 7 $\times$ 7 performed at low temperature in 2001 [27], this technique has been advanced to record multidimensional potential landscapes [28–32]. Assuming long-range (LR) electrostatic and van der Waals interactions are site independent, atomic interactions have been obtained by subtracting the extracted force with a fitted function of the LR force [29,33]. Such analyses are mostly acceptable in measurements on flat terraces, especially at small tip-surface separations because the atomic scale interaction dominates the potential variation. However near step edges, LR interactions are no longer site independent and hence can dominate the potential variation, especially with a larger tip-sample separation [34]. Identifying the origin of these LR interactions and interpreting their signatures in DFS measurements are important for characterizing these reactive sites, yet difficulties in extracting the signatures of these tiny force variations over a larger area remain a daunting task.

Here, we study this topic with a different approach, namely, the direct detection of the potential variation via the torsional frequency shift of the oscillating Si cantilever by bimodal DFM or DFS. Bimodal DFM with two resonance modes was originally incorporated in tapping mode to obtain higher resolution and less destructive measurement in air and liquids [35,36]. Instead of using two flexural modes, simultaneous detections of the vertical and lateral interactions have been demonstrated by using the torsional resonance mode. The site-independent interactions are invariant in the lateral directions so that they do not show up in the torsional signal [37]. Furthermore, the higher mechanical quality factor, compared to that of the flexural mode, can improve the force sensitivity itself [38]. Such extreme sensitivity to site-dependent interaction [39] allows us to measure the potential variations near the step edge of a prototype insulating ionic crystal LiF and investigate its changes with respect to an applied bias voltage. Our multiscale theoretical calculation concludes that the step ions are displaced by the electrostatic field by subpicometers. Consequently, the electrostatic forces from anion and cation are no longer damped at short range, and give rise to LR potential variation near the step edges.

All experiments were performed with our home-made ultrahigh vacuum DFM, operating at room temperature [40]. The potential variation of a stepped clean LiF (001) surface was measured with a commercially available Si cantilever (Nanosensor NCL-PPP) in bimodal operation mode [41], using the second flexural mode [42] and the torsional resonance [43]. The high effective stiffness $k_{2nd} = 1806$ N/m of the second mode realizes stable small amplitude operation of the vertical tip-sample interaction, which can reduce the averaging effect of the lateral force detection. Further details on the experiments are described in the supplementary material [44].

Figure 1(a) shows a topography of the LiF (001) surface, obtained at a constant vertical frequency shift $\Delta f_{ver} = -135$ Hz and a constant amplitude $A_{ver} = 400$ pm. The step runs through the middle of the image, but no other significant atomic feature was observed at this imaging distance. The corresponding line profile along A-A' reveals that the height of the step is approximately 230 pm, which is very close to the known monoatomic step height of LiF (001). In contrast, the simultaneous recorded Δf_{TR} signal, keeping the constant amplitude $A_{TR} = 150$, shows a stronger contrast at the vicinity to the step edge [Fig. 1(b)]. Since the dithering direction of the tip by the torsional mode is along the fast-scan X direction in this measurement (i.e., nearly perpendicular to the step run), the Δf_{TR} signal effectively corresponds to the lateral force gradient F'_X. From the corresponding line profile of the Δf_{TR} signal along B-B', we can also observe a more detailed structure of the step as the tip scans across the edge, originating from the Ehrlich-Schwoebel barrier: the negative Δf_{TR} on the lower terrace is caused by an attractive lateral force, and on the upper terrace the attraction gradually fades, bringing the frequency shift to zero. Since the interaction between the step edge and the tip has a vertical component, this feature would, in principle, be visible in the topography as well, but was completely hidden by the dominant van der Waals force. The decay lengths of Δf_{TR} on the two sides of the step are remarkably different, exhibiting a longer tail on the upper terrace, which cannot be explained in terms of purely short-range interactions. It is worth noting that although no significant contrast is observed in the topography, the atomic corrugation can be observed in the same Δf_{TR} image with a narrow contrast scale (-0.21–0.30 Hz) as shown in the right side of Fig. 1(b). This is due to the fact that the sensitivity of the Δf_{TR} signal to the site-dependent interaction (i.e., the short-range interaction on the flat surface) is extreme, as shown in our previous works [39].

In order to investigate the origin of the LR interaction, we performed bias spectroscopic measurements of the time-averaged cantilever deflection ΔZ_{def}, Δf_{ver}, and Δf_{TR} signals on the upper terrace near the step edge as indicated by a cross-marker in Fig. 1. For this measurement, the tip-sample distance was shifted farther away by 800 pm from the imaging distance, leading to an overall estimated distance of approximately 1 nm; the sample bias voltage was swept in the range of ± 6 V while the cantilever was electrically grounded. The results are shown in Fig. 2. Because of the small oscillation amplitude A_{ver}, the bias-induced capacitive interaction causes a small deflection, ΔZ_{def} [Fig. 2(a)]: a quadratic fit indicates that the contact potential difference (CPD) is -0.57 V. A clearer response to the bias voltage is visible in the Δf_{ver} signal [Fig. 2(b)]. Both channels clearly show a parabolic behavior, which is well known to be caused by the capacitive interaction. In the Δf_{ver} signal, we observed several jumps. These variations, consequently indicating different CPD values, are most likely due to a rearrangement of the ions in

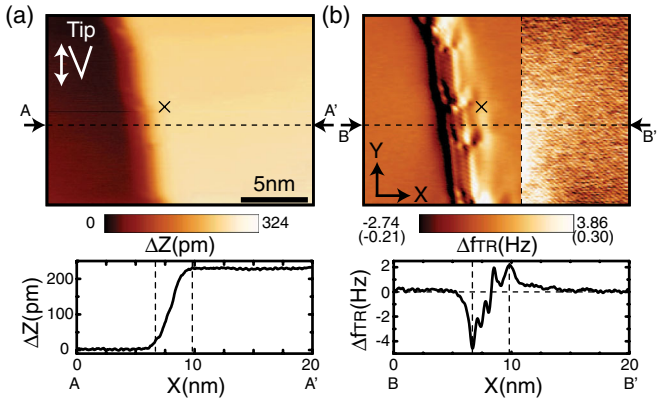

FIG. 1 (color online). Simultaneous DFM topography (a) and Δf_{TR} map (b) of LiF (001) near a monoatomic step with the respective line profiles: imaging area is 20×14 nm. Image contrast in the right part of (b) is enhanced to show the atomic corrugation (scale values are indicated in parentheses). The cross-marker shows the position chosen for bias spectroscopy.

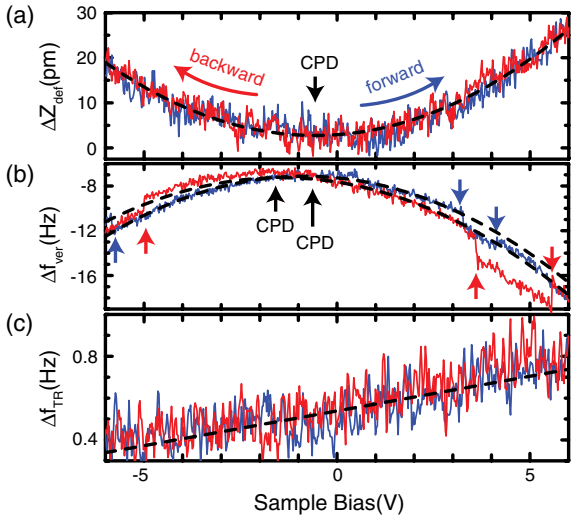

FIG. 2 (color online). Sample bias dependences of (a) ΔZ_{def}, (b) Δf_{ver}, and (c) Δf_{TR}, measured at $X = 6$ nm from the step edge and $Z = 1$ nm above the upper terrace. Blue and red lines represent the forward and backward scans, respectively.

the tip apex [45]. The CPD value is affected by the potential difference between tip and sample so that a differently charged tip apex results in the different CPD values as shown by the fitted quadratic functions with selected bias regions. However, since such a difference of the tip potential is not expected to induce site-dependent capacitive forces, similarly to applied bias voltage on flat terraces [37], it should cause no significant shift of the lateral signal Δf_{TR}, but surprisingly we observe a linear dependence on the bias [Fig. 2(c)].

In order to understand the observed LR feature and linear-bias dependence in the Δf_{TR} signal, we performed theoretical calculations with a virtual AFM using bimodal detection. Since the bias voltage is applied at the bottom of the thick LiF crystal ($t = 5$ mm), a single atomic scale calculation, including a few hundred atoms of the surface, cannot take into account the effect of such a thick dielectric material. On the other hand, a macroscopic calculation lacks the atomic scale details. To provide a correct description of the system, we built a multiscale model of the system, yielding the electrical properties at the macroscopic level and used the results as boundary conditions for an atomistic calculation-this is similar to a recent approach for including LR electrostatics into first-principles calculations [46]. Figure 3(a) shows the macroscopic setup, including the cantilever-tip assembly and the LiF sample; the electrostatic potential of this system is calculated with the finite element method [47,48], including the full thickness of the dielectric, as implemented in the commercial COMSOL package [49]. The generated field is then used as the boundary conditions for an atomistic calculation of a $Li_{910}F_{910}$ surface slab [see Fig. 3(b)], using the SCIFI code [50]. This approach allows us to include the influence of applied bias on the forces and atomic geometries. Interatomic interactions in the surface are included via fitted Buckingham potentials [51–54]. As the tip is contacted to the surface, we expect the apex to be covered by LiF and model it as a simple dipole [45,55,56]—since we are interested in the interactions at LR, an atomistic model of the tip is unnecessary. The resulting force field is then used to run our home-built virtual DFM [57] capable of simulating Δf_{TR} in the bimodal operation mode, enabling us to correlate the step atom displacements to the frequency shift as well as compare the latter to the experiment. Although this approach demonstrates good agreement with the experiment, the simulation suffers from the finite size effects of the atomistic model, causing the interaction energy to decrease as the tip is moved laterally and *runs out* of surface. Ultimately, this causes the frequency shifts to be systematically offset towards lower values, but this does not influence our conclusions. A detailed description of the different models can be found in the Supplemental Material [44].

The results show that the effective, *real* potential $\tilde{V}$ is directly proportional to the applied V_{bias} at the bottom of the sample, scaled down by a factor of approximately 0.4. Thus, an experimental bias range of $[-5, 5]$ volts corresponds roughly to $[-2, 2]$ volts applied to the electrode in the atomistic calculations. The bias voltage in the results shown hereafter accounts for the scaling. In the atomistic calculation, we placed the tip 2 nm laterally away from the step, at a tip-sample separation of 1 nm, which is a good estimation of the point where the bias spectroscopy was measured in the experiment. The simulated contrast, shown in Fig. 4(c), is directly proportional to the tip dipole, and it is found to be close to the experimental observation using 7 debye, which is reasonable in comparison with the dipoles of simple molecules and previous studies of polar

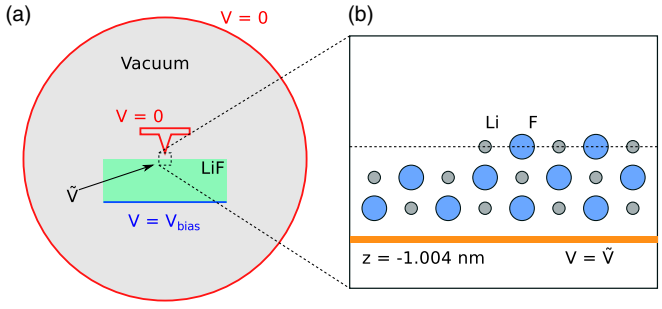

FIG. 3 (color online). (a) Schematic illustration of the macroscopic system used for FEM calculation (not in scale). The LiF slab is represented by the green box, while the electrodes are marked with red and blue lines, according to whether the applied potential is 0 or V_{bias}, respectively. (b) Atomistic model of the step edge with an auxiliary electrode kept at the effective potential.

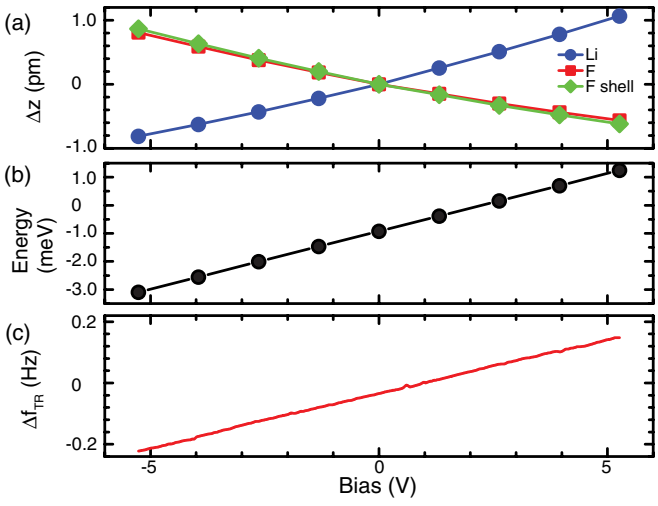

FIG. 4 (color online). (a) Displacements of step edge ions for different species relative to the initial configuration at $V = 0$: Li (blue circles), F (red squares), and F shells (green diamonds). (b) Interaction energy between the surface and the tip per unit of tip dipole. (c) Bias dependence of the torsional frequency shift calculated with a 7-debye tip dipole. The bias voltage values are scaled according to the calculation in the macroscopic model.

tips [45,55,56]. The origin of the simulated Δf_{TR} is found entirely in the atomic displacements of the step ions induced by the bias: the ions move mainly along the vertical direction by at most 2 pm [Fig. 4(a)]. The interaction energy between the surface atoms and the fixed dipole tip is plotted in Fig. 4(b), and since it is found to be directly proportional to the applied bias, it can be inferred that all its derivatives with respect to the lateral coordinate (namely, $F_x \approx dE/dx$ and $\Delta f_{TR} \approx dF_x/dx$) should also show the same linear dependence on the applied bias. The simulated Δf_{TR} is in qualitative and quantitative agreement with the experimental results as shown in Fig. 2(c). While no systematic error in forward and backward sweeps is observed, the signal-to-noise ratio in the measurement is not high. This is due to the fact that the oscillation amplitude in the torsional mode is much smaller than the optimal amplitude, which is related to the decay length of the interaction (for the upper terrace, $\lambda \approx 2.66\ \mathrm{nm}^{-1}$) [58]. Further improvement of the measurement by setting an optimal amplitude might reveal a more detailed potential landscape of the surface.

In summary, the detailed potential variation in the vicinity of a step of an ionic crystal was directly measured by bimodal DFM with the flexural and torsional resonance modes. The extreme sensitivity to the site-dependent interaction in the torsional signal revealed the extraordinary LR feature. Unambiguous agreement between experimental results and multiscale theoretical calculations demonstrates that the electrostatic field moves step atoms by subpicometers in different directions. It has been proven how in conventional KPFM the measured signal can be explained with a simple model, where the energy of the system comes mostly from the capacitive quadratic term in V [45] and the contribution from the ion-field coupling gives minor corrections [59]. With this work, both experimentally and theoretically, we show that the torsional mode is insensitive to the capacitor and the measured signal contains only information of the ion-field coupling, demonstrating how the lateral frequency shift is extremely sensitive to subpicometer changes in the ionic positions. This again emphasizes the power of multimode DFM techniques in increasing the quality and quantity of data extracted from a given experiment, and also promotes torsional resonance as a particularly sensitive probe of site-dependent interactions. Recently, the static charge distribution within a single molecule was measured by Kelvin force microscopy [60]. The presented sensitivity of the technique to small displacements could be critical for directly detecting the unveiled dynamics of configurational charge transfer within a molecule caused by an external electronic field.

This work was supported in part by the Swiss National Science Foundation, the ESF EUROCORE program FANAS and by the NCCR "Nanoscale Science" of the Swiss National Science Foundation. FFC, TH, and ASF wish to acknowledge the support from the Academy of Finland via its Centre of Excellence program and the Finnish Academy of Science and Letters, as well as the computational resources offered by CSC, Finland. The authors wish to thank A. Baratoff for useful discussions.

*shigeki.kawai@unibas.ch
†filippo.federici@tut.fi

[1] M. F. Crommie, C. P. Lutz, and D. M. Eigler, Nature (London) **363**, 524 (1993).
[2] J. Repp, G. Meyer, and K.-H. Rieder, Phys. Rev. Lett. **92**, 036803 (2004).
[3] M. Ono, Y. Nishigata, T. Nishio, T. Eguchi, and Y. Hasegawa, Phys. Rev. Lett. **96**, 016801 (2006).
[4] J. Repp, G. Meyer, S. M. Stojković, A. Gourdon, and C. Joachim, Phys. Rev. Lett. **94**, 026803 (2005).
[5] N. Pavliček, B. Fleury, M. Neu, J. Niedenführ, C. Herranz-Lancho, M. Ruben, and J. Repp, Phys. Rev. Lett. **108**, 086101 (2012).
[6] L. Nony, E. Gnecco, A. Baratoff, A. Alkauskas, R. Bennewitz, O. Pfeiffer, S. Maier, A. Wetzel, E. Meyer, and C. Gerber, Nano Lett. **4**, 2185 (2004).
[7] K. Lämmle, T. Trevethan, A. Schwarz, M. Watkins, A. Shluger, and R. Wiesendanger, Nano Lett. **10**, 2965 (2010).
[8] H.-J. Freund, Surf. Sci. **601**, 1438 (2007).
[9] T. König, G. H. Simon, U. Martinez, L. Giordano, G. Pacchioni, M. Heyde, and H.-J. Freund, ACS Nano **4**, 2510 (2010).
[10] F. Mohn, J. Repp, L. Gross, G. Meyer, M. S. Dyer, and M. Persson, Phys. Rev. Lett. **105**, 266102 (2010).
[11] M. A. Gosálvez, K. Sato, A. S. Foster, R. M. Nieminen, and H. Tanaka, J. Micromech. Microeng. **17**, S1 (2007).
[12] J. J. D. Yoreo, L. A. Zepeda-Ruiz, R. W. Friddle, S. R. Qiu, L. E. Wasylenki, A. A. Chernov, G. H. Gilmer, and P. M. Dove, Cryst. Growth Des. **9**, 5135 (2009).
[13] S. A. Burke, J. M. Mativetsky, R. Hoffmann, and P. Grütter, Phys. Rev. Lett. **94**, 096102 (2005).
[14] M. Fendrich and T. Kunstmann, Appl. Phys. Lett. **91**, 023101 (2007).
[15] S. Maier, L.-A. Fendt, L. Zimmerli, T. Glatzel, O. Pfeiffer, F. Diederich, and E. Meyer, Small **4**, 1115 (2008).
[16] C. R. Henry, Surf. Sci. Rep. **31**, 231 (1998).
[17] O. H. Pakarinen, J. M. Mativetsky, A. Gulans, M. J. Puska, A. S. Foster, and P. Grutter, Phys. Rev. B **80**, 085401 (2009).
[18] B. Such, T. Trevethan, T. Glatzel, S. Kawai, L. Zimmerli, E. Meyer, A. L. Shluger, C. H. M. Amijs, P. de Mendoza, and A. M. Echavarren, ACS Nano **4**, 3429 (2010).
[19] T. Filleter, W. Paul, and R. Bennewitz, Phys. Rev. B **77**, 035430 (2008).
[20] H. Hölscher, D. Ebeling, and U. D. Schwarz, Phys. Rev. Lett. **101**, 246105 (2008).
[21] R. Bennewitz, A. S. Foster, L. N. Kantorovich, M. Bammerlin, C. Loppacher, S. Schär, M. Guggisberg, E. Meyer, and A. L. Shluger, Phys. Rev. B **62**, 2074 (2000).
[22] R. L. Schwoebel and E. J. Shipsey, J. Appl. Phys. **37**, 3682 (1966).
[23] C. Barth and C. R. Henry, Nanotechnology **17**, S155 (2006).

[24] C. Barth and C. R. Henry, Phys. Rev. Lett. **98**, 136804 (2007).
[25] C. Barth, A. S. Foster, C. R. Henry, and A. L. Shluger, Adv. Mater. **23**, 477 (2011).
[26] T. R. Albrecht, P. Grütter, D. Horne, and D. Rugar, J. Appl. Phys. **69**, 668 (1991).
[27] M. A. Lantz, H. J. Hug, R. Hoffmann, P. J. A. van Schendel, P. Kappenberger, S. Martin, A. Baratoff, and H. J. Güntherodt, Science **291**, 2580 (2001).
[28] A. Schwarz, H. Hölscher, S. M. Langkat, and R. Wiesendanger, AIP Conf. Proc. **696**, 68 (2003).
[29] A. Schirmeisen, D. Weiner, and H. Fuchs, Phys. Rev. Lett. **97**, 136101 (2006).
[30] M. Ternes, C. P. Lutz, C. F. Hirjibehedin, F. J. Giessibl, and A. J. Heinrich, Science **319**, 1066 (2008).
[31] B. J. Albers, T. C. Schwendemann, M. Z. Baykara, N. Pilet, M. Liebmann, E. I. Altman, and U. D. Schwarz, Nature Nanotech. **4**, 307 (2009).
[32] S. Kawai, T. Glatzel, S. Koch, A. Baratoff, and E. Meyer, Phys. Rev. B **83**, 035421 (2011).
[33] R. Hoffmann, L. N. Kantorovich, A. Baratoff, H. J. Hug, and H. J. Güntherodt, Phys. Rev. Lett. **92**, 146103 (2004).
[34] M. Guggisberg, M. Bammerlin, A. Baratoff, R. Lüthi, C. Loppacher, F. Battiston, J. Lü, R. Bennewitz, E. Meyer, and H.-J. Güntherodt, Surf. Sci. **461**, 255 (2000).
[35] N. F. Martinez, S. Patil, J. R. Lozano, and R. García, Appl. Phys. Lett. **89**, 153115 (2006).
[36] J. R. Lozano and R. García, Phys. Rev. Lett. **100**, 076102 (2008).
[37] S. Kawai, N. Sasaki, and H. Kawakatsu, Phys. Rev. B **79**, 195412 (2009).
[38] O. Sahin, S. Magonov, C. Su, C. F. Quate, and O. Solgaard, Nature Nanotech. **2**, 507 (2007).
[39] S. Kawai, T. Glatzel, S. Koch, B. Such, A. Baratoff, and E. Meyer, Phys. Rev. B **81**, 085420 (2010).
[40] L. Howald, E. Meyer, R. Lüthi, H. Haefke, R. Overney, H. Rudin, and H. J. Güntherodt, Appl. Phys. Lett. **63**, 117 (1993).
[41] S. Kawai, T. Glatzel, S. Koch, B. Such, A. Baratoff, and E. Meyer, Phys. Rev. Lett. **103**, 220801 (2009).
[42] S. Kawai, S. Kitamura, D. Kobayashi, S. Meguro, and H. Kawakatsu, Appl. Phys. Lett. **86**, 193107 (2005).
[43] S. Kawai, S. Kitamura, D. Kobayashi, and H. Kawakatsu, Appl. Phys. Lett. **87**, 173105 (2005).
[44] See Supplemental Material at http://link.aps.org/supplemental/10.1103/PhysRevLett.109.146101 for further details on the experiments and theoretical calculations.
[45] T. Hynninen, A. S. Foster, and C. Barth, e-J. Surf. Sci. Nanotechnol. **9**, 6 (2011).
[46] A. Sadeghi, A. Baratoff, S. A. Ghasemi, G. Stefan, T. Glatzel, S. Kawai, and E. Meyer, Phys. Rev. B **86**, 075407 (2012).
[47] W. G. Strang and G. J. Fix, *An Analysis of the Finite Element Method* (Wellesley-Cambridge Press, Wellesley, MA, 1973).
[48] R. Ferrari, IEEE Antenn. Propag. Mag. **49**, 216 (2007).
[49] Sealing Technology **2010**, 4 (2010).
[50] L. N. Kantorovich, A. S. Foster, A. L. Shluger, and A. M. Stoneham, Surf. Sci. **445**, 283 (2000).
[51] R. A. Buckingham, Proc. R. Soc. A **168**, 264 (1938).
[52] B. G. Dick and A. W. Overhauser, Phys. Rev. **112**, 90 (1958).
[53] M. J. L. Sangster and R. M. Atwood, J. Phys. C **11**, 1541 (1978).
[54] A. L. Shluger, A. L. Rohl, D. H. Gay, and R. T. Williams, J. Phys. Condens. Matter **6**, 1825 (1994).
[55] M. Bieletzki, T. Hynninen, T. M. Soini, M. Pivetta, C. R. Henry, A. S. Foster, F. Esch, C. Barth, and U. Heiz, Phys. Chem. Chem. Phys. **12**, 3203 (2010).
[56] C. Barth, T. Hynninen, M. Bieletzki, C. R. Henry, A. S. Foster, F. Esch, and U. Heiz, New J. Phys. **12**, 093024 (2010).
[57] M. K. Rasmussen, A. S. Foster, B. Hinnemann, F. F. Canova, S. Helveg, K. Meinander, N. M. Martin, J. Knudsen, A. Vlad, E. Lundgren, A. Stierle, F. Besenbacher, and J. V. Lauritsen, Phys. Rev. Lett. **107**, 036102 (2011).
[58] F. J. Giessibl, Rev. Mod. Phys. **75**, 949 (2003).
[59] L. Nony, A. S. Foster, F. Bocquet, and C. Loppacher, Phys. Rev. Lett. **103**, 036802 (2009).
[60] F. Mohn, L. Gross, N. Moll, and G. Meyer, Nature Nanotech. **7**, 227 (2012).